https://doi.org/10.5194/gi-2022-24
Preprint. Discussion started: 24 January 2023

Geoscientific Instrumentation Methods and Data Systems Discussions

Sample labeling and classification method of hyperspectral remote sensing images based on texture features and semi-supervised learning

Ansheng Ye [1,2], Xiangbing Zhou [3,*], Yu Gong[4], Fang Miao[1], Huimin Zhao[4,*]

[1] *Key Lab of Earth Exploration & Information Techniques of Ministry Education, Chengdu University of Technology, Chengdu 610059, China*

[2]*School of Computer Science, Chengdu University, Chengdu 610106, China*

[3]*School of Information and Engineering, Sichuan Tourism University, Chengdu 610100, China*

[4] *College of Electronic Information and Automation, Civil Aviation University of China, Tianjin 300300, China*

*Corresponding author: zhouxb@uestc.edu.cn (Xiangbing Zhou); hm_zhao1977@126.com (Huimin Zhao)

Abstract

Hyperspectral images contain abundant spectral and spatial information about the earth's surface, labeling data processing and analysis more difficult, as well as the problem of sample labeling. In this paper, local binary pattern (LBP), sparse representation and mixed logistic regression model are introduced, and a sample labeling method based on neighborhood information and priority classifier discrimination is presented. Then, a hyperspectral remote sensing image classification method based on texture features and semi-supervised learning is implemented. The LBP is employed to extract features of spatial texture information from remote sensing images and enrich the feature information of samples. Then the multivariate logistic regression model is used to select the unlabeled samples with the largest amount of information, and the unlabeled samples with neighborhood information and priority classifier tags are selected to obtain the pseudo-labeled samples after learning. By making full use of the advantages of sparse representation and mixed logistic regression model, a new hyperspectral remote sensing image classification model based on semi-supervised learning is constructed to effectively achieve accurate classification of hyperspectral images. The data of Indian Pines, Salinas scene and Pavia University are selected to verify the validity of the proposed method. The experiment results show that the proposed classification method can obtain higher classification accuracy and show stronger timeliness and generalization ability.

Keywords: Hyperspectral remote sensing image; Local binary pattern; Sparse representation; Mixed logistic regression; Neighbourhood information

1. Introduction

Hyperspectral Image (HSI) is the simultaneous imaging of target areas in dozens to hundreds of continuous spectral bands. It effectively integrates the spatial and spectral information in the imaging scene, with strong target detection ability and better material identification ability (Chang et al., 2021; Chen et al., 2021; Dou et ai., 2020). It is widely used in agriculture and forestry, geological exploration, marine exploration, Environmental monitoring and other fields. However, HSI is characterized by high data dimension, large information redundancy and high correlation between bands, which brings great difficulties to its processing and classification (Dumke et al.,2019; Huang et al., 2020; Jiang et al., 2020; Seifi et al., 2017). Therefore, how to reduce the redundant information of the data, extract and use the features of the hyperspectral image effectively, and realize the accurate classification of the hyperspectral image are the hot and difficult issues in the current hyperspectral image processing and classification research.

Sample labeling of hyperspectral image data often requires expert knowledge and experience, so the cost of sample labeling is high(Shang et al., 2020). When the labeled samples are limited, semi-supervised learning can explore the useful information of the unlabeled samples to participate in the model training and reduce the labeling cost(Shi et al., 2019; Ye et al., 2021). In the field of machine learning, semi-supervised learning acquires knowledge and experience from a small number of labeled samples. Mining usable information from a large number of unlabeled samples helps the classification model to train and improve the classification accuracy (Yin et al., 2021; Yu et al., 2021; Chen et al., 2020). Therefore, a large number of scholars have carried out the research of semi-supervised learning in remote sensing images. Camps-Valls et al. (Camps-Valls et al., 2007) proposed a graph-based hyperspectral image classification method, and constructed the graph structure through the graph

https://doi.org/10.5194/gi-2022-24
Preprint. Discussion started: 24 January 2023

Geoscientific Instrumentation Methods and Data Systems Discussions
Open Access
EGU

method. The data context information is integrated based on the composite kernel and the Nystrom method is introduced to speed up classification. Yang et al. (Yang et al., 2012) proposed a semi-supervised band selection technique for hyperspectral image classification. A metric learning method is used to measure the features of hyperspectral images, and a semi-supervised learning method is used to select a subset of valid bands from the original bands. The validity of the method and the improvement of classification accuracy are verified by experiments. Tan et al. (Tan et al., 2014) proposed a hyperspectral image classification method based on segmentation integration and semi-supervised support vector machine. The spatial information of the tag samples is extracted using a segmentation algorithm to filter the samples, and then classified based on semi-supervised learning. Samiappan et al. (Samiappan et al., 2015) combined active learning and co-training to perform semi-supervised classification of hyperspectral images. The initial classification model is trained according to the labeled samples, and the heuristic active learning is performed on the unlabeled samples. Combined with the original data, the labeled sample set was divided into views, and the unlabeled samples with high heuristic values were selected to join the training sample set for co-training. Zhang (Zhang et al., 2016) used a semi-supervised classification method based on hierarchical segmentation and active learning to extract spatial information from hyperspectral images, then the training set is updated iteratively by using the information of a large number of unlabeled samples to complete the hyperspectral image classification.

In hyperspectral images, each pixel corresponds to a spectral curve that reflects its inherent physical, chemical and optical properties. The main basis of hyperspectral image classification is to use the feature information of different pixels to label the pixels belonging to different landmarks and obtain the corresponding classification maps (Zhang et al., 2022; Zhao et al., 2022). Therefore, a large number of scholars have carried out the research on hyperspectral image classification. Melgani et al. (Melgani et al., 2004) proposed a hyperspectral image classification method based on Support Vector Machines (SVM). The kernel function is introduced to solve the nonlinear separable problem and avoid the curse of dimensionality. Ratle et al. (Ratle et al., 2006) introduced neural networks into hyperspectral image classification. In the training phase, the loss function is optimized to avoid problems such as local optimization. Chen et al. (Chen et al., 2011) constructed a hyperspectral image classification model based on sparse representation, and compared the classification results of common machine learning methods. In order to improve the shortcomings of sparse representation in dealing with nonlinear problems, Chen et al. (Chen et al., 2013) introduced kernel method to propose a kernel sparse representation technique. In addition, Cui et al. (Cui et al., 2013) proposed a multiscale sparse representation algorithm for robust hyperspectral image classification. Automatic and adaptive weight allocation schemes based on spectral angle ratio are incorporated into the multi-classifier framework to fuse sparse representation information at all scales. Tang et al. (Tang et al., 2016) proposed two sparse representation algorithms based on manifolds to solve the instability problem of l1-based sparse algorithms. Using regularization and local invariance techniques, two manifold-based regularization items are merged into thel_1-based objective function. Wang et al. (Wang et al., 2016) applied the neighborhood-cutting technique to sparse representation, and combined the joint spatial and spectral sparse representation classification algorithm. Wang and Celik (Wang et al., 2018) improved the classification accuracy of hyperspectral images by combining context information in the sparse coefficient domain. Hu et al. (Hu et al., 2019) proposed two weighted kernel joint sparse representation methods, which determine the calculation weight by calculating the kernel similarity between adjacent pixels. The nearest neighbor regularization strategy is used to optimize both the weight of the projected adjacent pixels and the joint sparse representation factor. Xue et al. (Xue et al., 2017) presented two novel sparse graph regularization methods, SGR and SGR with total variation. Yang et al. (Yang et al., 2018) studied the effect of the p-norm distance metric on the minimum distance technique and proposes a supervised-learning p-norm distance metric to optimize the value of p. Zhang et al. (Zang et al., 2019) proposed a multi-scale dense network for HSI classification that made full use of different scale information in the network structure and combined scale information throughout the network. Liu et al. (Liu et al., 2021) proposed a class-wise adversarial adaptation in conjunction with the class-wise probability MMD as the class-wise distribution adaptation (CDA) network. Wang et al. (Wang et al., 2022) proposed graph-based semi-supervised learning with weighted features for HSI classification.

To sum up, hyperspectral images contain rich spectral and spatial information of earth surface features, which increases the difficulty of data processing and analysis. In addition, the training samples of actual hyperspectral images are small and there is a problem of sample labeling. The local binary pattern, sparse representation and mixed logistic regression model are used

https://doi.org/10.5194/gi-2022-24
Preprint. Discussion started: 24 January 2023

Geoscientific Instrumentation Methods and Data Systems Discussions

in this paper. A new hyperspectral image feature extraction method based on local binary pattern is proposed to obtain texture features of hyperspectral image samples and enrich hyperspectral image sample information. A sample selection strategy based on active learning is designed to determine the unlabeled samples. Based on this, a new sample labeling method based on neighbourhood information and priority classifier discrimination is deeply studied to expand the training samples. The hyperspectral remote sensing image classification method based on texture features and semi-supervised learning is studied to improve the classification accuracy of remote sensing images.

The main contributions of this paper are described as follows.

1) A novel a hyperspectral remote sensing image classification method based on texture features and semi-supervised learning is proposed, which introduces local binary pattern, sparse representation, hybrid logistic regression model and so on.

2) The local binary pattern is used to effectively extract the features of spatial texture information of remote sensing images and enrich the feature information of samples.

3) A multiple logistic regression model was used to optimally select unlabeled samples, which are labeled by using neighbourhood information and priority classifier discrimination to achieve pseudo-labeling of unlabeled samples.

4) A hyperspectral remote sensing image classification model based on semi-supervised learning is constructed to effectively achieve accurate classification of hyperspectral images by making full use of the advantages of sparse representation and mixed logistic regression model.

2. Basic methods

2.1. Local binary pattern (LBP)

LBP is a feature extraction method that extracts spatial texture information of images. Texture, which is widely used in image processing and image analysis, represents the slow change or periodic change of the surface structure of the object(Ojala et al. 1996). LBP is also widely used in feature extraction of hyperspectral images due to the simple structure and easy calculation. Give the center pixel $g_c(x_c, y_c)$ and the neighborhood pixel g_p,

$$g_p = (x_c + Rcos\left(\frac{2\Pi p}{P}\right), y_c - Rsin(\frac{2\Pi p}{P})) \quad (1)$$

where, $g_p(p = 0,1,...,P-1)$ represents the coordinate values of P pixels uniformly distributed on the circular domain with g_c as the centre and R as the radius. The local texture information at the center pixel is the circular area in the Figure 1, which can be represented.

7		...		28
	79	26	78	
	132	68	10	
	30	202	252	
24		...		59

Figure1. The quantized texture feature form of one region

$$LBP_{g_c} = 2^p \times \sum_{p=0}^{P-1} s(g_p - g_c) \quad (2)$$

$$s(x) = \begin{cases} 1, x > 0 \\ 0, x \le 0 \end{cases} \quad (3)$$

2.2. Sparse expression

Sparse representation means that the signal can be approximately represented by a linear combination of the atoms in the dictionary. Now, $X = [X_1, X_2, ..., X_c] \in R^D$ is given as the HSI pixel and D is the number of image bands. In here, $X_i = [x_{i1}, x_{i2}, ..., x_{iN_c}] \in R^D$, N_c represents the number of samples in class i.

https://doi.org/10.5194/gi-2022-24
Preprint. Discussion started: 24 January 2023

Geoscientific Instrumentation Methods and Data Systems Discussions

For samples in class i, it can be approximated as follow.

$$\begin{aligned} y &\approx x_{i1}\alpha_1 + x_{i2}\alpha_2 + \ldots + x_{iN_c}\alpha_{N_c} \\ &= \left[x_{i1}, x_{i2}, \ldots, x_{iN_c}\right]\left[\alpha_1, \alpha_2, \ldots, \alpha_{N_c}\right]^T \\ &= X_i\alpha_i \end{aligned} \tag{4}$$

where, X_i represents a sparse sub-dictionary of the samples in class i. α_i represents the sparse vector of test samples y, which contains only a few non-zero values.

In order to obtain the sparsest vector α_i, the following formula is solved.

$$\tilde{\alpha} = \arg\min \left\|\alpha_i\right\|_0, s.t. y = A\alpha_i \tag{5}$$

where, $\|.\|_0$ is a l_0 norm, which represents the number of non-zero atoms in the vector, also known as sparsity. A is a sparse dictionary. It is a NP-hard problem to solve the formula directly. Under some conditions, the minimization solving problem(l_0) is approximated by the minimization solving problem(l_1), which can be relaxed.

$$\tilde{\alpha} = \arg\min \left\|\alpha_i\right\|_1, s.t. y = A\alpha_i \tag{6}$$

Furthermore, the solution can be converted to the following formula.

$$\tilde{\alpha} = \arg\min \left\|\alpha_i\right\|_0, s.t. \left\|A\alpha_i - y\right\|_2^2 < \varepsilon \tag{7}$$

where, ε represents the refactoring error. Orthogonal matching pursuit (OMP) algorithm can be used to solve the above equation. After the sparsity coefficient is calculated, the reconstruction residual for each class of the test sample y can be calculated.

$$r_i(y) = \left\|y - A\tilde{\alpha}_i\right\|_2 \tag{8}$$

where, $i \in \{1, 2, ..., C\}$.

Finally, the reconstruction residuals of all category dictionaries are compared. The minimum residual is the category y.

$$class(y) = \arg\min(r_i(y)), i = 1, 2, ...C \tag{9}$$

3. An image sample labeling method based on neighbourhood information and priority classifier discrimination

3.1. Sample selection method based on multiple logistic regression model

Before the samples are labeled, sample selection is required. This is because if all unlabeled samples are labeled directly, all unlabeled samples need to be labeled, which will cost a lot of computational cost. Moreover, due to the small number of initial labeled samples and the limited information available, it is difficult to label some samples with a certain accuracy. Mislabeled samples obviously affect the classification accuracy of the model. The main objective of the sample selection strategy is to select the unlabeled samples with the largest amount of information. These unlabeled samples can construct a valuable training set after labeling, and effectively promote the improvement of classification results. Therefore, a kind of information selection method based on multiple logistic regression model is proposed to realize the selection of samples.

That is to say, the classified probability matrix $p\left(y_i^k | x_i\right)$ of each sample by using multiple logistic regression model has a large amount of information that can be mined as the initial data. The multiple logistic regression classifier is modeled by discriminant Bayesian decision model. According to the theory of generalized linear model, it can be obtained as follow.

$$P(y;\delta) = b(y)\exp\left(\delta^T T(y) - a(\delta)\right) \tag{10}$$

The specific form of multiple logistic regression is described as follow.

$$p(y_i = k | x_i, \eta) = \exp\left(\eta^k g(x_i)\right) \Big/ \sum_{k=1}^{N} \exp\left(\eta^k g(x_i)\right) \tag{11}$$

where, $g(x) = [g_1(x), g_2(x), \ldots, g_f(x)]^T$ is the feature vectors of the input, and $\eta = [\eta_1^T, \eta_2^T, \ldots \eta_k^T]$ represents the regression parameter vector of the classifier. It is worth noting that the feature vector is often represented by introducing the

https://doi.org/10.5194/gi-2022-24
Preprint. Discussion started: 24 January 2023

Geoscientific Instrumentation Methods and Data Systems Discussions

idea of kernel, which is not only used to improve the indivisibility, but also helps the classifier to fit better by training samples. Generally, the kernel function is radial basis function (RBF) as follow.

$$K(x_m, x_n) = e^{\frac{-||x_m - x_n||^2}{2p^2}} \tag{12}$$

After the feature vector is determined, the regression parameter η of model is only determined, and then the probability matrix $p(y_i^k|x_i)$ of each unlabeled sample belonging to each class is determined. The amount of information of the samples is determined by the Breaking Ties (BT) and the Least Confidence (LC). In this paper, the BT method is selected to determine the amount of information.

The BT method shows the similarity between the two categories by comparing the difference between the maximum category probability and the sub-maximum category probability. The difference is smaller, the similarity between the two types of samples is greater. The uncertainty is greater, the amount of information is greater. S_i is used to indicate the similarity between categories. The formula is described as follow.

$$S_i = maxp(y_i^k|x_i) - secondmax(p(y_i^k|x_i)) \tag{13}$$

The S_i is finally sorted in ascending order.

3.2. A sample labeling method based on neighborhood information and priority classifier

The features of hyperspectral images have some correlation. The ground objects are closer, the correlation is stronger. In the research of sample labeling, spatial neighborhood information based on training samples is widely used. However, due to the unknown central pixel and the lack of sufficient determination information, the neighborhood information of unlabeled samples is relatively less in the research of sample labeling. Generally, the label of any pixel on a hyperspectral image must be consistent with the label of one pixel in its neighborhood. This property can be applied to label the unlabeled samples. The label information of training samples around the unlabeled samples can be used to discriminate the unlabeled samples. The labeling discrimination method based on neighborhood information centers on the sample to be labeled. The labeled samples appearing around it are labeled with a block diagram. All the occurrences of sample labels are recorded and denoted as the neighborhood information set. Then, the labeled samples are used as training samples to train the classifier and classify the unlabeled samples. Determine whether the predicted sample label by the classifier appears in the neighborhood information set of the unlabeled samples. If it appears, the predicted label by the classifier is the sample label. Otherwise, the samples are put to be labeled back into the unlabeled sample set. One of the most important problems is whether the unlabeled samples which satisfy the neighborhood information can be reliably labeled by the classifier. At present, some studies use multiple classifiers to discriminate together and achieve good classification effect. However, a problem is how to determine the determination of labels, when the predicted labels by multiple classifiers are inconsistent, but all appear in the neighborhood information set of unlabeled samples.

Therefore, a sample labeling method based on priority classifier discrimination is proposed in this paper. For unlabeled samples with the neighborhood information, the classifier with the highest priority is used for prediction. If the obtained prediction marker appears in the neighborhood information set, its marker is determined. Otherwise, the classifier with the lowest priority is used for prediction. Then judge whether the label can be determined until the end of the sample labeling. The sample labeling method based on neighborhood information and priority classifier discrimination is shown in Figure 2.

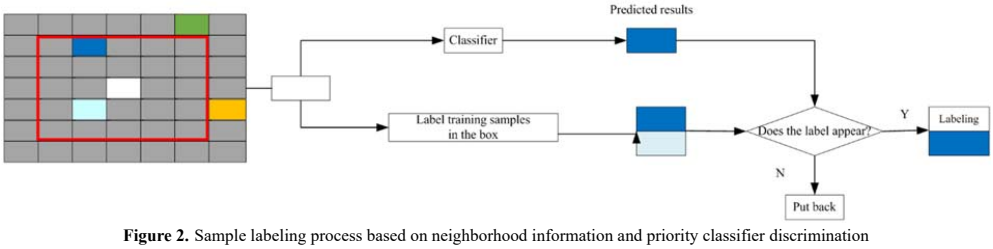

Figure 2. Sample labeling process based on neighborhood information and priority classifier discrimination

This labeling method is a cyclical iterative process. Although it is not possible to ensure enough training samples around all unlabeled samples at the initial stage of sample labeling, it can ensure that some unlabeled samples are sufficient. The unlabeled

https://doi.org/10.5194/gi-2022-24
Preprint. Discussion started: 24 January 2023

Geoscientific Instrumentation Methods and Data Systems Discussions

samples are then labeled and extended to the training set. With each iteration, the training set grows. Those unlabeled samples whose neighborhood training samples are not sufficient may reach the label condition at a certain labeling time. This sample labeling method with replacement ensures the accuracy of sample labeling to a certain extent, and improves the performance of classifier step by step.

4. Hyperspectral image classification method based on texture features and semi-supervised learning

4.1. The idea of hyperspectral image classification

Hyperspectral images consist of pairs of continuous spectral bands, which contain rich spectral and spatial information of earth surface features. So that some objects that cannot be identified by conventional remote sensing means can be identified in hyperspectral images. However, the abundant data information increases the difficulty of data processing and analysis, and there are problems such as the difficulty of sample labeling. In order to improve the accuracy of hyperspectral image classification, a new hyperspectral image classification method based on texture features and semi-supervised learning is proposed in this paper. Firstly, aiming at the problems of high correlation between bands, information redundancy, high data dimension and complex processing, LBP is employed to deal with the hyperspectral images. The texture features of hyperspectral images are effectively extracted to enrich the feature information of samples. Then, to solve the problem of limited label samples, a new sample labeling method based on neighborhood information and priority classifier is proposed. And a sample selection strategy is designed to find some samples from a large number of unlabeled samples. Secondly, the selection samples are labeled by using the neighborhood information and the priority classifier. Finally, the classifier is applied to achieve accurate classification of hyperspectral images.

4.2. The model of hyperspectral image classification

The hyperspectral image classification model based on texture features and semi-supervised learning is shown in Figure 3.

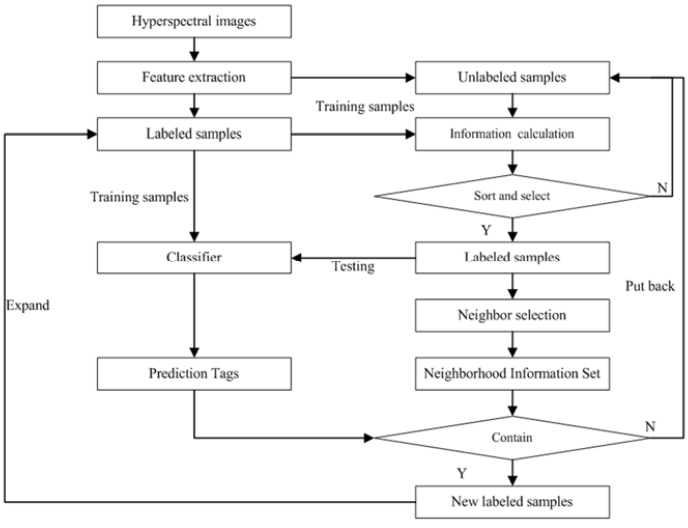

Figure 3. Hyperspectral image classification model based on texture features and semi-supervised learning

5. Case analysis

5.1. Experimental data

(1) Indian Pines data

The images of Indian pines in northwest Indiana were collected by AVIRIS sensor. The images consist of 145×145 pixels and 224 spectral reflection bands with a wavelength range of 0.4~2.5 nm, including 16 types of feature elements. The false color map and real ground object distribution are shown in Figure 4.

https://doi.org/10.5194/gi-2022-24
Preprint. Discussion started: 24 January 2023

Geoscientific Instrumentation Methods and Data Systems Discussions

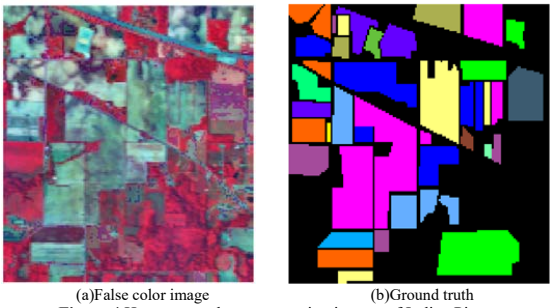

(a)False color image (b)Ground truth

Figure 4 Hyperspectral remote sensing images of Indian Pines

(2) Salinas Scene data

The AVIRIS spectrometer collects images of the Salinas Valley in California, USA, with a size of 512×217 pixels and a total of 224 bands. After removing the bands covering the water absorption area, 204 bands were used, including 16 types of ground feature elements. The false color map and the real ground object distribution are shown in Figure 5.

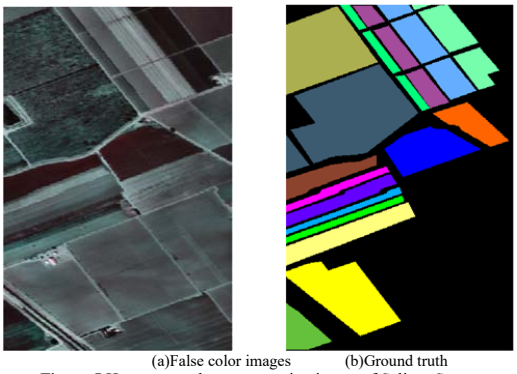

(a)False color images (b)Ground truth

Figure 5 Hyperspectral remote sensing image of Salinas Scene

(3) Pavia University data

Images of the Italian University of Pavia campus taken by the Rosis Spectrometer. It is 610 × 340 pixels in size and has a total of 115 wavebands. The 103 wavebands after removing the wavebands covering the water-absorbing region contain a total of 9 types of features. The false color map and the real ground object distribution are shown in Figure 6.

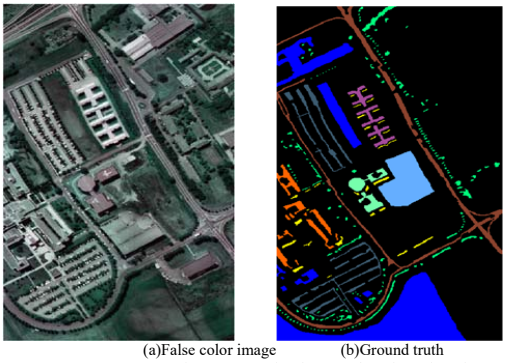

(a)False color image (b)Ground truth

Figure 6 Hyperspectral remote sensing image of Pavia University

In the experiment, 10% of each type of ground object of the three kinds of data is randomly selected as the training samples, and the rest is the test samples.

https://doi.org/10.5194/gi-2022-24
Preprint. Discussion started: 24 January 2023

Geoscientific Instrumentation Methods and Data Systems Discussions

5.2. Evaluation criteria

Confusion Matrix (CM) is usually used in the classification and evaluation of hyperspectral images. A confusion matrix is generally defined as follow.

$$P = \begin{bmatrix} p_{11} & p_{12} & \cdots & p_{1n} \\ p_{21} & p_{22} & \cdots & p_{2n} \\ \cdots & \cdots & \cdots & \cdots \\ p_{n1} & p_{n2} & \cdots & p_{nn} \end{bmatrix} \tag{14}$$

where, n denotes the number of objects in the category, p_{ij} represents the number of samples belonging to class i that were assigned to class j. The total amount of data in each row denotes the true number of objects in that category. The total amount of data for each column represents the total number of samples.

Based on the confusion matrix, three classification indexes can be obtained, which are Overall Accuracy (OA), Average Accuracy (AA) and Kappa coefficient.

$$OA = \frac{\sum_{i=1}^{n} p_{ii}}{N} \tag{15}$$

where, N represents the total number of samples participating in the classification. p_{ii} represents the number of correctly classified samples of class i. It represents the probability that the classified result corresponds to its true label for each random sample.

$$CA_i = \frac{p_{ii}}{N_i} \tag{16}$$

where, N_i represents the total number of samples for the first category in class i. CA_i represents the probability that category i is correctly classified.

$$Kappa = \frac{(n(\sum_{i=1}^{N} p_{ii}) - \sum_{i=1}^{N}(\sum_{j=1}^{N} p_{ij} \sum_{j=1}^{N} p_{ji}))}{n^2 - \sum_{i=1}^{N}(\sum_{j=1}^{N} p_{ij} \sum_{j=1}^{N} p_{ji})} \tag{17}$$

The Kappa coefficient comprehensively considers the number of objects correctly classified and the error of being misclassified on the diagonal of the confusion matrix.

5.3. Parameter determination and analysis

5.3.1 Sample selection methods

The quality of sample selection directly affects the efficiency of the whole experiment, and also affects the performance of classifier. In order to select the best sample selection method, the experimental results of IE, ME, BT and LC on three kinds of hyperspectral images were compared. The experiment is set to take 10 initial samples for each class, and all remaining samples are test samples. Two hundred unlabeled samples were selected by four sample selection methods in each iteration, and the real labels were given to the unlabeled samples. The samples were used to expand the training set, train the classifier and classify the test samples. The quality of the sample selection method is determined according to the classification results after each iteration is executed. The classification accuracy of different sample selection methods on different data sets is shown in Table 1.

Table 1 The classification accuracy of different methods on different data sets(%)

Data	Selection method	1	2	3	4	5	6	7	8	9	10
Indian Pines	IE	78.39	79.10	79.99	80.71	82.11	83.47	84.10	85.51	86.48	87.23
	ME	80.33	86.83	91.08	92.92	95.28	97.02	98.00	98.45	98.90	99.13
	BT	**91.47**	**95.47**	**98.22**	**98.36**	**98.64**	**98.59**	**98.66**	**98.71**	**99.34**	**99.29**
	LC	84.74	88.95	91.63	94.33	95.27	96.46	98.15	98.55	98.62	98.66
Pavia University	IE	69.87	71.31	71.75	71.74	72.04	72.40	73.25	73.36	73.76	74.45
	ME	73.01	75.23	78.74	82.78	89.14	92.82	95.14	96.10	**97.13**	**97.82**
	BT	**87.54**	**92.63**	**94.51**	**95.24**	**95.84**	**96.10**	**96.39**	**96.50**	96.69	96.71
	LC	74.91	76.33	80.76	84.45	87.23	89.89	90.27	90.67	90.56	91.47
Salinas Scene	IE	84.16	84.60	84.65	85.02	85.09	85.25	85.50	85.65	85.91	85.98
	ME	85.14	89.29	92.81	94.31	96.48	97.41	98.04	98.20	98.66	98.88

https://doi.org/10.5194/gi-2022-24
Preprint. Discussion started: 24 January 2023

Geoscientific Instrumentation Methods and Data Systems Discussions

	BT	**95.30**	**96.98**	**98.26**	**98.71**	**98.95**	**98.90**	**99.03**	**99.21**	**99.25**	**99.24**
	LC	88.60	91.19	92.84	93.58	93.80	95.74	97.56	97.72	98.56	98.86

From Table 1, it can be seen that the classification accuracies of ME, BT and LC are greatly improved with the increase of the number of iterations on the three data sets. The results of the BT method are significantly better than those of the other methods. The accuracy can be improved to a high level in the first few iterations, indicating that BT method can select samples with greater classification improvement. Therefore, the BT method is chosen as the sample selection method in this paper.

5.3.2 Determination of sample size

In the labeling process, the samples are not completely labeled correctly. The more samples are screened, the more samples may be misclassified. This will make the training set more noisy and affects the generalization ability of the classifier. If the number of samples is too small, the number of labeled samples will not be enough to improve the classification accuracy of the classifier or will reduce the classification efficiency. The results of classification accuracy under different sample sizes are shown in Table 2.

Table 2 The classification accuracy results under different sample sizes(%)

Data	Quantity	1	2	3	4	5	6	7	8	9	10
Indian Pines	200	77.30	77.57	78.32	77.97	78.59	78.97	78.96	79.28	**79.51**	79.23
	400	77.54	78.60	79.80	80.80	82.13	82.20	83.03	83.77	83.83	**83.85**
	600	77.52	79.54	79.37	79.27	80.08	81.99	83.89	83.60	84.30	**84.48**
	800	77.75	79.84	80.87	80.22	82.11	83.91	84.41	84.57	85.12	**85.94**
	1000	77.85	80.49	80.28	82.74	81.35	82.60	84.18	85.88	86.77	**87.84**
	1200	77.85	79.95	79.79	80.38	81.59	84.41	84.72	85.74	87.48	**88.85**
	1400	78.18	80.20	80.09	83.96	85.00	85.78	87.93	89.90	91.07	**91.20**
	1600	78.55	80.56	80.59	84.12	86.90	87.82	89.02	90.87	91.49	**91.83**
	1800	78.34	79.76	79.23	82.64	85.39	87.32	88.81	89.97	90.69	**91.46**
	2000	78.01	79.16	80.24	82.55	86.02	87.48	88.66	89.63	90.02	**90.46**
Pavia University	200	68.75	73.93	76.73	78.18	79.23	80.92	81.85	82.40	82.74	**83.60**
	400	66.41	73.11	75.45	78.20	81.18	82.13	82.57	83.39	**84.07**	83.98
	600	68.88	76.35	78.22	80.73	82.59	83.29	83.68	84.57	84.95	**84.98**
	800	69.89	77.50	80.31	81.91	83.22	84.85	84.99	84.79	85.16	**85.31**
	1000	70.28	76.35	79.92	82.68	83.83	84.48	84.84	85.21	**85.37**	85.04
	1200	70.24	75.18	80.32	83.13	84.14	85.04	85.30	**85.55**	85.04	84.90
	1400	70.34	76.23	80.57	82.46	83.92	84.71	85.59	85.77	85.87	**86.47**
	1600	70.40	75.87	80.64	83.06	83.93	84.69	85.28	86.02	**86.19**	85.83
	1800	69.77	76.12	80.18	82.99	85.19	85.04	84.89	85.26	**85.68**	85.68
	2000	69.71	75.90	82.29	83.40	84.41	85.23	85.59	85.77	85.86	**85.87**
Salinas Scene	200	85.09	87.26	89.04	**89.35**	89.24	89.22	88.85	88.47	88.14	88.03
	400	84.94	88.34	**89.88**	89.26	89.12	88.88	88.26	87.68	87.40	87.25
	600	85.69	**90.85**	90.80	90.42	89.71	89.04	88.63	87.84	87.12	86.60
	800	85.36	**89.17**	88.87	87.96	87.46	86.85	86.42	85.69	85.13	84.58
	1000	85.35	88.93	89.88	**89.04**	88.34	87.58	87.03	85.49	85.08	85.08
	1200	85.04	89.66	**90.08**	88.98	87.67	87.14	86.13	85.30	85.09	84.85
	1400	85.07	88.46	**89.39**	88.63	88.10	88.06	87.34	86.81	86.69	86.58
	1600	85.47	89.54	**89.88**	88.87	87.68	86.21	85.00	84.34	83.89	83.70
	1800	85.50	**90.16**	90.15	89.45	88.58	87.71	86.79	86.52	86.31	85.93
	2000	85.48	**89.40**	89.38	88.60	87.73	85.98	85.67	85.12	85.39	85.34

https://doi.org/10.5194/gi-2022-24
Preprint. Discussion started: 24 January 2023

Geoscientific Instrumentation Methods and Data Systems Discussions
Open Access
EGU

It can be seen from Table 2 that the selection of sample screening quantity in different data sets presents different rules. Indian Pines datasets have the highest classification accuracy after 10 iterations are finished. Pavia University datasets has the highest classification accuracy after 8,9, and 10 iterations are finished. Salinas Scene datasets have the highest classification accuracy after 2,3, and 4 iterations are finished. The sample screening quantity with the highest accuracy is regarded as the experimental parameter, which were 1600 for Indian Pines, 1400 for Pavia University and 600 for Salinas Scene.

5.3.3 Determination of block window size

The size of the block window determines the neighborhood information set of the samples, which directly affects the accuracy of the pseudo-tagging method. Due to the different scale of data sets, the optimal block window size is also determined by a large number of experiments. The classification accuracy under different block window sizes is shown in table 3.

Table 3 The classification accuracy (%) under different block window sizes

Data	Block window size	1	2	3	4	5	6	7	8	9	10
Indian Pines	3	77.62	77.86	78.35	78.65	78.91	79.14	79.09	79.12	**79.56**	**79.56**
	4	77.73	78.24	78.65	78.75	78.70	78.66	79.14	79.18	79.70	**79.74**
	5	78.41	79.61	79.41	81.28	81.11	81.73	82.67	82.84	84.18	**84.68**
	6	77.85	80.14	80.41	80.91	80.90	83.54	84.91	85.09	86.42	**88.30**
	7	78.86	80.58	82.58	84.90	86.55	86.99	88.47	88.87	89.58	**90.98**
	8	78.33	78.95	81.00	84.24	85.44	86.37	87.60	88.13	88.57	**89.19**
	9	79.61	81.00	83.39	85.51	85.71	86.34	86.78	86.86	87.07	**87.86**
	10	78.61	79.32	83.45	85.45	85.59	85.69	86.12	87.00	87.17	**87.32**
Pavia University	5	68.39	68.38	68.38	68.38	68.38	68.38	68.38	68.38	68.38	68.38
	10	68.20	67.67	69.05	69.06	68.30	68.13	68.06	67.98	67.89	67.62
	15	70.91	70.59	70.96	70.50	71.89	73.54	**73.80**	74.58	75.25	75.32
	20	71.47	71.63	73.60	76.12	75.99	75.61	77.18	77.51	77.81	**78.14**
	25	71.25	74.57	78.52	79.15	81.95	82.32	83.66	84.88	85.45	**85.51**
	30	70.28	76.35	79.92	82.68	83.83	84.48	84.84	85.21	**85.37**	85.04
	35	71.48	77.43	80.15	81.75	83.18	83.62	**84.11**	83.65	83.23	83.17
	40	73.40	77.50	80.36	81.92	**83.15**	82.68	82.23	82.38	82.18	82.04
Salinas Scene	5	83.94	83.94	83.94	83.94	83.94	83.94	83.94	83.94	83.94	83.94
	10	83.61	84.16	84.95	85.03	84.77	84.68	84.59	84.82	84.61	**85.48**
	15	83.86	83.17	85.51	87.04	87.70	88.44	89.77	89.60	91.01	**91.09**
	20	84.16	86.84	89.41	90.56	90.22	90.69	91.02	**91.13**	90.87	90.68
	25	84.11	88.22	89.46	**89.68**	89.35	88.77	87.86	87.49	86.71	86.78
	30	85.35	**88.93**	89.88	89.04	88.34	87.58	87.03	85.49	85.08	85.08
	35	86.17	**88.80**	88.67	87.67	86.63	85.84	85.26	84.87	83.95	83.06
	40	86.86	**89.25**	89.02	87.78	86.37	84.74	83.60	82.83	81.69	80.92

As can be seen from Table 3, different datasets present different changes in classification accuracy. Compared with the other two data sets, the scale of Indian Pines is the smallest, so its experimental block window side length values from 3 to 10. With

https://doi.org/10.5194/gi-2022-24
Preprint. Discussion started: 24 January 2023

Geoscientific Instrumentation Methods and Data Systems Discussions
Open Access
EGU

the increase of the number of iterations, the classification accuracy showed a trend of gradual increase, and the optimal accuracy was obtained when the side length was 7. When the side length of the block window for Pavia and Salinas datasets is too small, the classification accuracy will not improve with the increase of iteration times. This indicates that the neighborhood information set cannot help the sample to distinguish the category at this time.

With the increase of the side length of the block window, the number of iterations to achieve the optimal classification accuracy is advanced, but the optimal accuracy decreases. The block window is larger, the more noise information will be introduced, and that will affect the accuracy of sample labeling. Therefore, the block window size of the Indian Pines dataset is 7 * 7, and the block window sizes of the Pavia and Salinas datasets are 25 * 25 and 20 * 20, respectively.

5.3.4 Determination of priority classifier

In fact, the determination of pseudo-tags of samples mainly depends on the determination of classifiers, KNN, SRC, NRS, MLR are employed to determine the pseudo-tags. The experimental results of single classifier and combination of different classifiers on different data sets are shown in Table 4 ~ Table 6.

Table 4 The experimental results of different classifier combinations in Indian Pines data set

Classifier	Index	1	2	3	4	5	6	7	8	9	10
KNN	NUM	314	673	1139	1630	2178	2680	3324	4063	4820	5474
	OA(%)	78.69	79.93	81.20	82.05	82.49	84.38	85.70	86.52	87.33	87.77
SRC	NUM	311	648	1068	1525	2032	2606	3248	3899	4668	**5522**
	OA(%)	78.64	80.42	80.10	81.56	82.87	84.39	85.83	87.04	87.92	88.19
NRS	NUM	315	673	1116	1597	2136	2697	3265	3815	4437	5016
	OA(%)	78.82	81.02	80.96	83.71	84.94	85.57	86.87	88.01	89.25	**89.42**
MLR	NUM	133	295	580	936	1296	1790	2396	3077	3858	4648
	OA(%)	77.55	79.31	82.21	83.91	83.99	85.75	87.36	87.68	88.27	88.41
KNN+SRC	NUM	317	706	1120	1702	2294	2967	3728	4494	5233	5950
	OA(%)	78.71	80.96	81.99	83.97	84.96	85.82	86.99	87.75	87.93	88.10
KNN+NRS	NUM	317	707	1198	1691	2308	2954	3625	4450	5374	6305
	OA(%)	78.78	80.27	80.73	82.51	83.82	85.45	87.56	89.06	89.95	90.19
KNN+MLR	NUM	318	712	1206	1794	2555	3398	4292	5072	5783	6678
	OA(%)	78.79	80.56	82.57	86.08	87.10	87.87	88.50	88.88	89.18	89.31
SRC+KNN	NUM	317	706	1134	1673	2223	2875	3658	4317	5011	5748
	OA(%)	78.71	81.09	81.51	83.17	84.27	85.84	86.94	87.54	88.26	88.64
SRC+NRS	NUM	318	730	1205	1778	2372	3091	3969	4813	5787	6641
	OA(%)	78.81	80.79	82.37	85.03	86.81	88.45	88.93	89.86	90.49	90.78
SRC+MLR	NUM	315	708	1153	1744	2457	3322	4231	5042	5800	6735
	OA(%)	78.80	80.92	82.16	85.16	86.24	87.61	88.39	88.71	89.07	89.19
NRS+KNN	NUM	317	707	1202	1712	2385	3021	3700	4538	5399	6333
	OA(%)	78.74	80.67	81.33	83.36	84.46	86.35	87.93	89.23	90.03	90.43
NRS+SRC	NUM	318	734	1207	1728	2378	3061	3959	4799	5691	6739
	OA(%)	78.77	81.01	82.56	84.52	86.37	87.43	88.95	90.11	90.61	90.90
NRS+MLR	NUM	318	694	1148	1690	2446	3194	4102	4950	5768	6792
	OA(%)	78.91	81.39	81.62	85.51	87.21	89.63	90.28	90.92	91.28	91.88
MLR+KNN	NUM	318	677	1166	1689	2429	3246	4018	4737	5677	6672
	OA(%)	78.30	81.13	81.85	85.94	87.22	88.28	88.77	88.98	89.20	89.29
MLR+SRC	NUM	315	704	1258	1741	2439	3286	4097	4867	5775	6760
	OA(%)	78.31	81.81	82.55	85.09	86.86	88.30	89.01	89.44	90.21	90.71
MLR+NRS	NUM	318	683	1154	1701	2458	3301	4219	5057	5997	**6889**
	OA(%)	78.46	81.49	82.11	86.14	87.86	89.70	90.68	91.58	92.15	**92.42**

From the experimental results on the Indian Pines dataset, it can draw the following conclusions. With the increase of iterations, the classification accuracy of each sample increased gradually. Compared with the results of the single classifier, the SRC has the largest number of samples after 10 iterations are finished, but the classification effect is not the best. The classifier

https://doi.org/10.5194/gi-2022-24
Preprint. Discussion started: 24 January 2023

Geoscientific Instrumentation Methods and Data Systems Discussions

with the best classification effect is NRS. The number of samples and classification accuracy of the combination of two groups of classifiers are mostly better than that of a single classifier. The experimental results are different for two groups of classifiers with different priority. The classifier with NRS can achieve more than 90% classification effect after 10 iterations are finished. The number of combinations with MLR was more than 6600 after 10 iterations are finished, and the best combination was MLR + NRS after 10 iterations are finished.

Table 5 The experimental results of different classifiers for Pavia University data

Classifier	Index	1	2	3	4	5	6	7	8	9	10
KNN	NUM	236	444	661	965	1210	1466	1812	2254	2762	3251
	OA(%)	71.19	73.36	74.70	75.69	76.10	76.16	77.28	78.48	77.60	77.69
SRC	NUM	225	477	733	1080	1492	2047	2793	3654	4605	5631
	OA(%)	72.21	72.19	76.97	79.12	80.08	81.77	83.09	84.07	84.95	85.27
NRS	NUM	225	438	763	1007	1256	1487	1726	1893	1991	2179
	OA(%)	71.22	73.74	75.14	76.59	76.15	76.47	76.41	76.20	75.68	75.40
MLR	NUM	100	244	396	605	829	1035	1304	1587	1872	2183
	OA(%)	72.36	76.37	77.18	79.04	79.40	81.16	82.21	82.18	83.36	**85.85**
KNN+SRC	NUM	248	473	787	1118	1509	1996	2552	3111	3975	4837
	OA(%)	71.48	72.82	74.61	76.59	78.38	80.08	80.82	81.62	82.40	83.99
KNN+NRS	NUM	240	491	775	1067	1382	1850	2403	3040	3794	4415
	OA(%)	71.11	73.83	77.44	78.83	79.50	79.58	79.39	80.11	80.74	81.48
KNN+MLR	NUM	244	515	822	1176	1616	2162	2905	3698	4745	5682
	OA(%)	71.37	75.03	77.84	78.08	79.73	79.59	81.30	83.88	84.90	85.08
SRC+KNN	NUM	248	476	795	1215	1725	2298	3055	3967	4977	5913
	OA(%)	71.38	72.54	75.26	78.09	79.19	80.21	81.88	83.31	83.35	83.51
SRC+NRS	NUM	242	511	867	1385	1889	2513	3201	3988	4910	5794
	OA(%)	71.40	74.12	77.56	80.80	82.19	82.55	83.02	83.80	84.34	85.09
SRC+MLR	NUM	236	507	841	1289	1731	2261	3016	3928	4939	6015
	OA(%)	71.52	73.62	76.47	78.45	79.51	81.54	83.10	84.37	84.68	84.66
NRS+KNN	NUM	240	486	803	1119	1541	1992	2557	3190	3939	4611
	OA(%)	71.05	74.37	76.57	77.77	78.06	77.21	76.75	77.35	78.88	79.28
NRS+SRC	NUM	242	501	803	1296	1792	2433	3089	3839	4776	5798
	OA(%)	71.44	74.50	76.72	79.93	81.44	81.90	82.85	83.81	85.00	85.48
NRS+MLR	NUM	234	517	828	1237	1796	2446	3354	4220	5061	5857
	OA(%)	71.49	75.47	77.89	80.86	83.68	84.43	84.93	85.12	85.57	85.46
MLR+KNN	NUM	244	486	746	1170	1658	2300	3205	4208	5336	**6514**
	OA(%)	71.47	75.30	76.67	78.76	80.35	82.97	85.05	86.05	86.88	87.02
MLR+SRC	NUM	236	504	903	1310	1708	2207	3009	4024	5098	6234
	OA(%)	71.71	74.01	79.30	79.81	80.40	83.03	86.27	86.93	87.97	**88.53**
MLR+NRS	NUM	234	524	787	1205	1738	2374	3116	3953	4754	5586
	OA(%)	71.63	75.94	79.83	80.66	82.75	84.64	85.98	86.19	86.37	86.87

As can be seen in Table 5, compared with the experimental results by single classifier, the number of labeled samples with SRC is the largest after 10 iterations are finished, which is higher than the other three methods. However, the MLR obtained best classification results. After 10 iterations are finished, the number of labeled samples of the two classifiers is more than that of the single classifier. With KNN, SRC and NRS as the first priority classifiers, the classification results of the sample set after 10 iterations are not as good as those obtained by using MLR. The combination of MLR as the first priority classifier has better classification effect than single MLR after 10 iterations are finished.

Table 6 The experimental results of different classifiers for Salinas Scene data

Classifier	Index	1	2	3	4	5	6	7	8	9	10
KNN	NUM	133	251	443	684	963	1304	1672	2047	2425	2857
	OA(%)	83.38	86.46	86.46	86.65	87.26	87.31	87.79	87.92	87.66	87.15

https://doi.org/10.5194/gi-2022-24
Preprint. Discussion started: 24 January 2023

Geoscientific Instrumentation Methods and Data Systems Discussions

SRC	NUM	144	275	441	666	937	1255	1606	1968	2391	2811
	OA(%)	83.10	83.56	85.11	85.83	85.81	86.63	86.50	86.64	86.95	86.96
NRS	NUM	148	271	423	668	952	1263	1569	1940	2351	2799
	OA(%)	84.04	86.06	87.62	87.63	87.10	87.48	88.44	88.43	88.32	87.92
MLR	NUM	102	177	302	451	621	867	1176	1518	1848	2217
	OA(%)	82.88	85.41	87.11	88.36	88.73	90.68	91.52	92.20	91.70	92.02
KNN+SRC	NUM	146	294	479	694	976	1330	1691	2106	2520	2985
	OA(%)	83.60	84.65	85.38	86.76	87.39	87.39	88.00	88.11	87.53	87.23
KNN+NRS	NUM	150	297	500	761	1108	1466	1891	2354	2834	3316
	OA(%)	83.53	86.43	87.14	87.49	87.64	87.37	88.06	88.03	87.95	88.03
KNN+MLR	NUM	143	285	508	768	1132	1546	2026	2526	3049	3590
	OA(%)	83.38	85.50	86.34	88.35	88.80	90.07	90.24	90.08	89.86	89.79
SRC+KNN	NUM	146	287	472	686	957	1281	1673	2061	2485	2892
	OA(%)	83.25	84.70	85.79	85.88	86.70	86.92	86.89	86.93	86.85	86.90
SRC+NRS	NUM	150	280	493	755	1017	1328	1708	2114	2539	2982
	OA(%)	83.07	85.55	86.28	85.47	86.66	86.97	87.52	87.05	87.19	87.16
SRC+MLR	NUM	150	271	483	720	1108	1499	1958	2451	2969	3487
	OA(%)	83.15	84.27	87.25	87.88	88.88	89.29	89.36	89.85	89.70	89.85
NRS+KNN	NUM	150	298	519	814	1148	1556	2037	2538	3027	3522
	OA(%)	84.01	87.12	87.79	87.30	87.54	88.38	88.09	88.25	87.95	87.88
NRS+SRC	NUM	150	284	488	803	1158	1539	1988	2482	2955	3423
	OA(%)	83.91	87.23	86.98	87.73	88.30	88.97	89.57	89.57	89.60	89.43
NRS+MLR	NUM	153	293	509	762	1104	1509	1940	2441	2934	3452
	OA(%)	83.87	85.82	88.25	89.93	90.40	90.51	90.75	90.48	90.12	89.61
MLR+KNN	NUM	143	299	521	825	1187	1602	2046	2514	2993	3407
	OA(%)	82.80	85.42	87.67	88.79	89.68	90.06	90.54	90.92	91.27	91.32
MLR+SRC	NUM	150	292	521	799	1123	1537	2007	2448	2929	3367
	OA(%)	82.91	85.45	88.89	90.12	90.21	90.93	90.99	91.83	92.08	**92.64**
MLR+NRS	NUM	153	315	564	841	1197	1605	2064	2561	3060	3500
	OA(%)	82.81	84.87	88.16	89.34	89.69	90.03	90.42	90.52	91.19	91.43

For Salinas Scene data, the number of labeled samples by MLR after 10 iterations is the smallest, but the classification accuracy of the labeled samples is the highest. After 10 iterations are finished, the number of iterations of the two classifiers is also higher than that of the single classifier. However, from the perspective of the performance of labeled samples in classification, MLR+SRC has higher classification results than MLR, which indicates that the addition of classifiers does not necessarily improve the classification accuracy, and experiments and analysis are needed for different data sets.

From the three experiments, it can be seen that the method with the largest number of labeled samples does not necessarily achieve the best classification results. The labeled samples are needed to improve the classification accuracy of the classifier, so the obtained labeled samples after 10 iterations are taken as the evaluation criteria. The Indian Pines data set uses a combination of classifiers MLR + NRS. The Pavia University and Salinas Scene data sets use MLR + SRC.

5.4. Experimental results and analysis

Based on the above analysis, the related parameters are shown in Table 7.

Table 7 The parameter settings

Data set	Indian Pines	Pavia University	Salinas Scene
Selection policy	BT	BT	BT
Number of selections	1600	1400	600
Window size	7*7	25*25	20*20
Combination of classifiers	MLR+NRS	MLR+SRC	MLR+SRC
Number of labeled samples	6889	6234	3367

https://doi.org/10.5194/gi-2022-24
Preprint. Discussion started: 24 January 2023

Geoscientific Instrumentation Methods and Data Systems Discussions
Open Access
EGU

Firstly, the local binary pattern is used to extract the features of spatial texture information of hyperspectral remote sensing images. Secondly, the sample labeling method based on neighborhood information and priority classifier is proposed to obtain the learned pseudo-labeled samples. Then the SRC classifier is trained with the labeled samples, and the test samples are predicted. The obtained classification results are compared with those obtained by the SRC classifier on the initial training data, and the classification results of training models with different training data are shown in Table 8.

Table 8 The classification results of training models with different training data

Training samples	Index	Initial samples	Labeling samples
Indian Pines	AA	67.93%	84.70%
	OA	77.38%	92.42%
	KAPPA	0.746	0.914
Pavia University	AA	60.53%	81.87%
	OA	69.00%	88.53%
	KAPPA	0.609	0.848
Salinas Scene	AA	82.59%	87.76%
	OA	84.00%	92.64%
	KAPPA	0.823	0.918

The classification visualizations of the classification model for the initial samples and labeled samples are shown in Figure 7 and Figure 8.

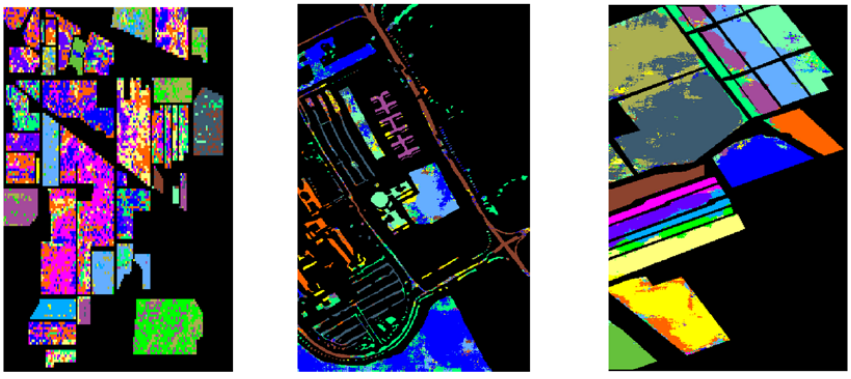

(a)Indian Pines (b)Pavia University (c)Salinas Scene

Figure 7 The classification results of the initial samples

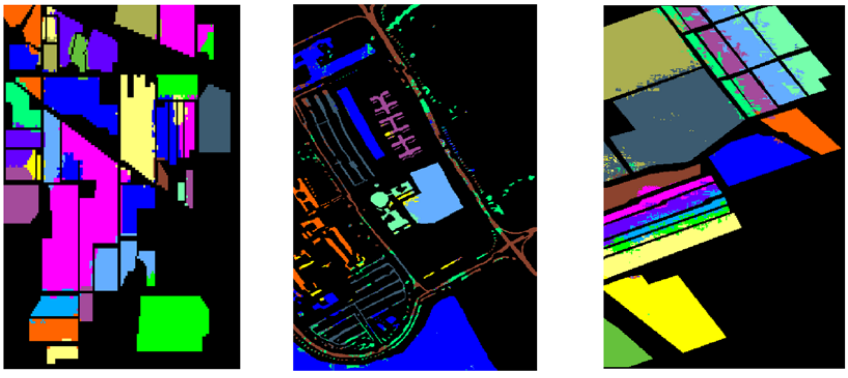

(a)Indian Pines (b)Pavia University (c)Salinas Scene

Figure 8 The classification results of the labeling samples

https://doi.org/10.5194/gi-2022-24
Preprint. Discussion started: 24 January 2023

Geoscientific Instrumentation Methods and Data Systems Discussions

By comparing with the results of the experiments, it is not difficult to find that the classification results of the classifier trained with expanded samples on the three sets of data are better than those of the classifier trained with initial samples. Moreover, from the classification visualization, it can see that the obtained classification results by the classifier and the labeled samples is smoother and has fewer discrete points, which indicates that the generalization ability of the classifier is improved by labeling the samples.

6. Conclusion

For the difficulties of hyperspectral image processing and analysis, a hyperspectral remote sensing image classification method based on texture features and semi-supervised learning is implemented by introducing local binary model, sparse representation and mixed logistic regression model. The local binary pattern is employed to deal with the hyperspectral data and extract the texture features of the hyperspectral remote sensing image. A sample labeling method based on neighborhood information and priority classifier is proposed to obtain the learned pseudo-labeled samples. The problem of limited labeled samples of hyperspectral images is solved. The data of Indian Pines, Salinas scene and Pavia University are selected in here. The experiment results of the BT method are obviously better than those of other methods. The block window of Indian Pines dataset is 7*7. The block windows of Pavia University and Salinas scene are 25 * 25 and 20 * 20, respectively. The combination of MLR and SRC can get better classification results. The obtained classification results by the classifier and the labeled samples are smoother and has fewer discrete points, which indicates that the generalization ability of the classifier is improved by labeling the samples from the classification visualization.

Author Contributions

Conceptualization, Ansheng Ye and Xiangbing Zhou; Methodology, Ansheng Ye and Yu Gong; Software, Yu Gong.; Validation, Fang Miao and Yu Gong; Resources, Fang Miao; Writing—original draft preparation, Ansheng Ye and Yu Gong; Writing—review and editing, Xiangbing Zhou and Huimin Zhao; Visualization, Fang Miao; Project administration, Huimin Zhao; Funding acquisition, Xiangbing Zhou. All authors have read and agreed to the published version of the manuscript.

Acknowledgments

This research was funded by the Sichuan Science and Technology Program, grant number 2019ZYZF0169, 2019YFG0307, 2021YFS0407; the A Ba Achievements Transformation Program, grant number R21CGZH0001; the Chengdu Science and technology planning project, grant number 2021-YF05-00933-SN.

Data Availability Statement

Not applicable

Conflicts of Interest

The authors declare no conflict of interest.

References

Camps-Valls G, Bandos T, Zhou D. (2007). Semi-supervised graph-based hyperspectral image classification. IEEE Transactions on Geoscience and Remote Sensing, 45(10):3044-3054.

Chang C, Kuo Y, Chen S, Liang C, Ma KY, Hu PF. (2021). Self-Mutual information-based band selection for hyperspectral image classification. IEEE Trans Geoscience and Remote Sensing, 59 (7): 5979-5997.

Chen, HY, Fang M, Xu S. (2020). Hyperspectral remote sensing image classification with CNN based on quantum genetic-optimized sparse representation. IEEE Access, 8: 99900-99909.

Chen H, Miao F, Chen Y. (2021). A hyperspectral image classification method using multifeature vectors and optimized KELM. IEEE Journal of Selected Topics in Applied Earth Observations and Remote Sensing, 14: 2781-2795.

https://doi.org/10.5194/gi-2022-24
Preprint. Discussion started: 24 January 2023

Geoscientific Instrumentation Methods and Data Systems Discussions

Chen Y, Nasser MN, Tran TD. (2011). Hyperspectral image classification using dictionary-based sparse representation. IEEE Transactions on Geoscience and Remote Sensing, 49(10):3973-3985.

Chen Y, Nasser MN, Tran TD. (2013). Hyperspectral image classification via kernel sparse representation. IEEE Transactions on Geoscience and Remote Sensing, 51(1):217–231.

Cui M, Prasad S. (2013).Multiscale sparse representation classification for robust hyperspectral image analysis. IEEE Global Conference on Signal and Information Processing, 969-972.

Dou Z, Gao K, Zhang X, Wang H, Han L. (2020). Band selection of hyperspectral images using attention-based autoencoders. IEEE Geoscience and Remote Sensing Letters, 18 (1): 147-151.

Dumke I, Ludvigsen M, Ellefmo SL, Søreide F, Johnsen G, Murton B. (2019). Underwater hyperspectral imaging using a stationary platform in the transatlantic geotraverse hydrothermal field. IEEE Transactions on Geoscience and Remote Sensing, 57 (5): 2947-2962.

Huang W, Huang Y, Wang H, Liu Y, Shim HJ. (2020). Local binary patterns and superpixel-based multiple kernels for hyperspectral image classification. IEEE Journal of Selected Topics in Applied Earth Observations and Remote Sensing, 13: 4550-4563.

Hu S, Xu C, Peng J, Yan X, Long T. (2019).Weighted Kernel joint sparse representation for hyperspectral image classification. IET Image Processing, 13(2):254-260.

Jiang X, Liu W, Zhang Y, Liu J, Li S, Lin J. (2020). Spectral-spatial hyperspectral image classification using dual-channel capsule networks. IEEE Geoscience and Remote Sensing Letters, 18 (6): 1094-1098.

Liu ZX, Ma L, Du Q. (2021).Class-wise distribution adaptation for unsupervised classification of hyperspectral remote sensing images. IEEE Transactions on Geoscience and Remote Sensing, 59(1): 508-521

Melgani F, Bruzzone L. (2004). Classification of hyperspectral remote sensing images with support vector machines. 2004. IEEE Transactions on Geoscience and Remote Sensing, 42(8):1778-1790.

Ojala T, Harwood I. (1996).A comparative study of texture measures with classification based on feature distributions. Pattern Recognition29(1):51-59.

Ratle, Terrettaz-Zufferey, Kanevski, et al. (206). Learning manifolds in forensic data. international conference on artificial neural networks. Springer, Berlin, Heidelberg.

Samiappan S, Moorhead R J. (2015). Semi-supervised co-training and active learning framework for hyperspectral image classification.2015 IEEE International Geoscience and Remote Sensing Symposium(IGARSS), IEEE:401-404.

Seifi M, Ghassemian H. (2017). A probabilistic SVM approach for hyperspectral image classification using spectral and texture features. International Journal of Remote Sensing, 38 (15): 4265-4284.

Shang X, Song M, Chang CI. (2020). An iterative random training sample selection approach to constrained energy minimization for hyperspectral image classification. IEEE Geoscience and Remote Sensing Letters, 18 (9): 1625-1629.

Shi C, Pun CM. (2019). Multiscale superpixel-based hyperspectral image classification using recurrent neural networks with stacked autoencoders. IEEE Transactions on Multimedia, 22 (2): 487-501.

Tan K, Li E, Qian D, et al. (2014). An efficient semi-supervised classification approach for hyperspectral imagery. ISPRS Journal of Photogrammetry & Remote Sensing,, 97:36-45.

Tang YY, Yuan H, Li L. (2014).Manifold-based sparse representation for hyperspectral image classification. IEEE Transactions on Geoscience and Remote Sensing, 52(12):7606-7618.

Wang C, Wang H, Hu B, Jia W, Xu J, Li X. (2016). A novel spatial-spectral sparse representation for hyperspectral image classification based on neighborhood segmentation. Spectroscopy and Spectral Analysis, 36(9):2919-2924.

Wang HR, Celik T. (2018). Sparse representation-based hyperspectral image classification. Signal Image and Video Processing, 12(5):1009-1017.

Wang QY, Zhang Q, Zhang JP, Kang SQ, Wang YJ. (2022). Graph-based semisupervised learning with weighted features for hyperspectral remote sensing image classification. IEEE Journal of Selected Topics in Applied Earth Observations and Remote Sensing, 15: 6356-6370

Xue ZH, Du PJ, Li J, Su HJ. (2017). Sparse graph regularization for hyperspectral remote sensing image classification. IEEE Transactions on Geoscience and Remote Sensing, 55(4): 2351-2366

Yang C, Liu S C, Bruzzone L, et al. (2012). A semisupervised feature metric-based band selection method for hyperspectral image classification. Hyperspectral Image and Signal Processing (WHISPERS), 2012 4th Workshop on. IEEE.

Yang M, Li CH, Guan J, Yan XS. (2018). A supervised-learning p-norm distance metric for hyperspectral remote sensing image classification. IEEE Geoscience and Remote Sensing Letters, 15(9): 1432-1436

Ye X, Ma J, Xiong H. (2021). Local affine preservation with motion consistency for feature matching of remote sensing images. IEEE Transactions on Geoscience and Remote Sensing, 60: 1-12.

https://doi.org/10.5194/gi-2022-24
Preprint. Discussion started: 24 January 2023

Geoscientific Instrumentation Methods and Data Systems Discussions

Yin J, Qi C, Chen Q, Qu J. (2021). Spatial-spectral network for hyperspectral image classification: A 3-D CNN and Bi-LSTM framework. Remote Sensing, 13 (12), 2353.

Yu C, Zhou S, Song M, Chang CI. (2021). Semisupervised hyperspectral band selection based on dual-constrained low-rank representation. IEEE Geoscience and Remote Sensing Letters, 19: 1-5.

Zhang CJ, Li GD, Du SH. (2019). Multi-scale dense networks for hyperspectral remote sensing image classification. IEEE Transactions on Geoscience and Remote Sensing, 57(11): 9201-9222

Zhang J, Meng Z, Zhao F, Liu H, (2022). Chang Z. Convolution transformer mixer for hyperspectral image classification. IEEE Geoscience and Remote Sensing Letters, doi:10.1109/LGRS.2022.3208935.

Zhao XD, Zhang MM, Tao R, Li W, Liao WZ, Tian LF, Philips W. (2022). Fractional Fourier image transformer for multimodal remote sensing data classification. IEEE Transactions on Neural Networks and Learning Systems, doi: 10.1109/TNNLS.2022.3189994

Zhang Z, Crawford M. (2016). Semi-supervised multi-metric active learning for classification of hyperspectral images.2016 IEEE International Geoscience and Remote Sensing Symposium(IGARSS), IEEE:1843-1847.